Optical spectroscopy of high-L Rydberg states of argon

L. E. Wright, E. L. Snow,* and S. R. Lundeen
Department of Physics, Colorado State University, Fort Collins, Colorado 80523, USA

W. G. Sturrus
Department of Physics, Youngstown State University, Youngstown, Ohio 44555, USA

(Received 7 November 2006; published 5 February 2007)

High-L fine structure patterns in $n=9$ and $n=17$ Rydberg levels of argon have been studied using a Doppler-tuned CO_2 laser and a fast beam of argon atoms. Analysis of the measured pattern using the polarization model yields the scalar dipole polarizability and quadrupole moment of the $^2P_{3/2}$ Ar^+ ion. The results are $\alpha_S = 6.83(8)a_0^3$ and $Q=-0.5177(15)ea_0^2$. Within the precision of this study, no vector component of the structure was observed.

DOI: 10.1103/PhysRevA.75.022503 PACS number(s): 32.10.Dk, 32.10.Fn, 32.30.Bv

I. INTRODUCTION

Nonpenetrating high-L ($L \geqslant 5$) Rydberg states of atoms display fine structure patterns determined by weak long-range interactions between the Rydberg electron and the electrons within a positive ion core. These interactions break the degeneracy among high-L levels that would characterize a purely hydrogenic system. From measurements of these fine structure patterns, properties of the core ion can be extracted. So far, there have been few experimental studies of these patterns, since these states are difficult to measure with conventional spectroscopic methods and a wide range of high-L states must be included to establish the pattern. Resonant excitation Stark ionization spectroscopy (RESIS) provides a means to accomplish this in a variety of systems [1]. Studies in He [2], Ne [3], N [4], and Ba [5] using the RESIS method have been used to determine properties of their respective core ions, such as their dipole polarizabilities and quadrupole moments. This method has also been used to determine these same properties of the core ions of the molecules H_2 [6,7] and D_2 [7]. Recently, the same method has been used to measure the polarizabilities of the Si^{2+} [8] and Si^{3+} [9] ions by the study of fine structure patterns in Rydberg ions. In many cases, the properties of the core ion determined by this method achieve a level of precision that challenges the best calculations.

Measurements of the fine structure in Rydberg states of argon are interesting since the $^2P_{3/2}$ Ar^+-ion core is not spherically symmetric and thus has a permanent quadrupole moment. This gives rise to a tensor fine structure pattern consisting of four energy levels for each value of L. Patterns of this type have been observed in only a few cases, N^+ [4], H_2^+ [6], and Ne^+ [3]. The most precise measurements, made in neon, showed that in addition to the scalar and tensor interactions between the Rydberg electron and the ion core, small vector interactions were also present. This is partly due to magnetic interactions and partly due to nonadiabatic electric interactions. These vector interactions, especially the nonadiabatic electric interaction, which has been named "vector hyperpolarizability"[10], have attracted significant theoretical interest [11,12]. Since argon and neon have similar electronic structure and since nonadiabatic effects generally increase for heavier atoms, studies of the argon fine structure could reveal larger contributions of this type.

The fine structure spectra of argon Rydberg states observed in this experiment are the transitions between the $n=9$ and $n=17$ states. All the transitions observed were those with $J_C=3/2$, where J_C is the total angular momentum of the core ion. The transitions observed were those with angular momentum states $L \geqslant 5$ and governed by the selection rules $\Delta L = \pm 1$ and $\Delta K = \pm 1$ or 0, where $K=J_C+L$ is the total angular momentum of the atom. The spin of the Rydberg electron is ignored, since the splittings of the energy levels due to electron spin are very small and were unresolved in this experiment. In this discussion, individual states are identified with the notation nL_K.

II. EXPERIMENT

The apparatus used for this study is shown schematically in Fig. 1. A 9.5-keV Ar^+-ion beam was created using a Colutron ion source. The argon ion was selected by means of a $\vec{v} \times \vec{B}$ velocity filter. The ion beam then passed through a Rydberg target, a thermal Rb beam excited by three cw lasers to the $9F$ state. Through collisions between the argon ions and the $9F$ Rb atoms, a charge exchange occurs for a small percentage of the ions, creating neutral Rydberg atoms of argon. The beam then passes through an initial stripper, which Stark ionizes states greater than $n \geqslant 15$ and deflects any remaining argon ions. This creates a neutral beam with a significant population in the $n=9$ state. The beam then enters the laser interaction region, where it is intersected by a CO_2 laser, which excites the $n=9$ atoms to the $n=17$ states. The laser frequency is Doppler tuned in the atom's rest frame by changing the angle of intersection between the laser and the beam. The beam then passes through another Stark ionizer, where the $n=17$ state atoms are ionized and then deflected into a detector.

The CO_2 laser is set, depending on the transition to be observed, to the $10R(18)$ or $10R(20)$ lines (974.6219 cm^{-1} and 975.9304 cm^{-1}, respectively), which are close to the hydrogenic frequency, 975.0545 cm^{-1}, of the $n=9$ to the n

*Current address: Department of Physics, State University of New York Fredonia, Fredonia, NY 14063.

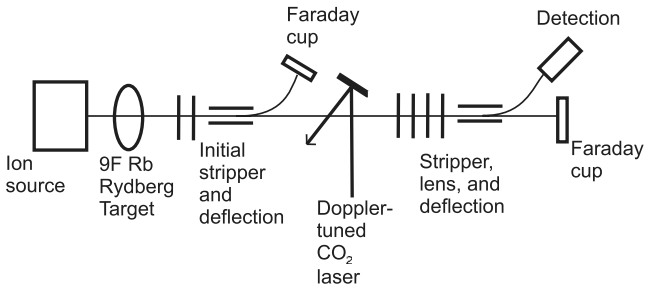

FIG. 1. Schematic of the apparatus used for this study. A 9.5-keV Ar^+ beam is created in a Colutron ion source and then passes through a $9F$ Rb Rydberg target, where some of the argon ions capture an electron. The beam then passes through an initial stripper, which ionizes states $n>15$ and deflects all Ar^+ into a Faraday cup. The neutral argon Rydberg atom beam is then intersected by a Doppler-tuned CO_2 laser, which excites the $n=9$ atoms to a particular state in $n=17$. The atoms again pass through a Stark ionizer, where any atoms excited to the $n=17$ state are ionized, focused by a lens, and then deflected into a channeltron for detection. The remaining neutral atoms are collected in a Faraday cup.

$=17$ transition in the argon Rydberg atom. The laser beam reflects off a mirror that is mounted on a rotating stage. By rotating the mirror, the angle of intersection between the laser and the argon beam can be changed, allowing for various transitions to be excited. The Doppler-tuned laser frequency is given by

$$\nu' = \frac{\nu_L}{\sqrt{1-\beta^2}}\{1+\beta\sin[2(\theta_{stage}-\theta_{perp})]\}, \qquad (1)$$

where ν_L is the fixed laser frequency, ν' is the Doppler-shifted laser frequency, $\beta=v/c$ is the speed of the argon beam, θ_{stage} is the angle reading on the rotation stage, and θ_{perp} is the angle reading on the stage when the laser beam is perpendicular to the argon beam. A typical resonance signal,

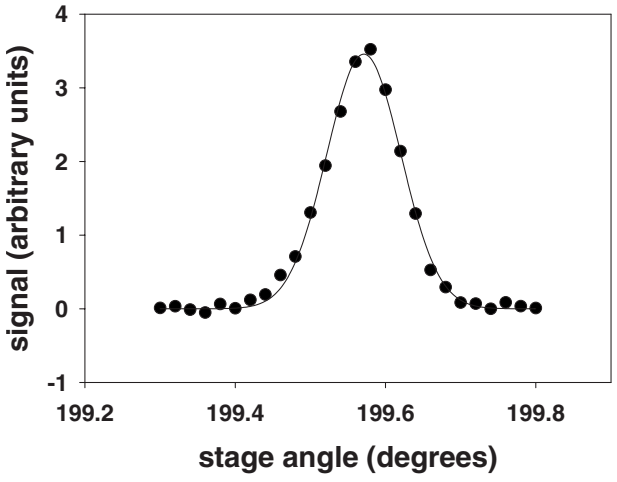

FIG. 2. Typical resonance signal obtained using the RESIS optical method. The current is measured versus the reading on the rotation stage where the CO_2 laser intersects the argon beam. This one is of the $9K_{13/2}$-$17L_{15/2}$ transition. The error for each point is comparable to the size of the data point.

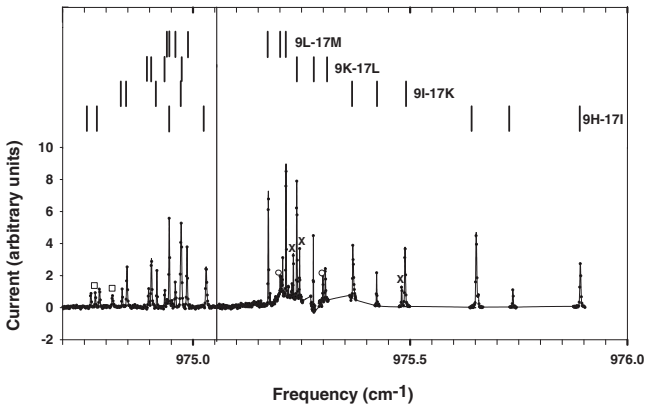

FIG. 3. The observed spectrum of the $n=9$ to the $n=17$ transitions in argon Rydberg atoms, as a plot of the Doppler-tuned CO_2 laser frequency vs signal current. The lines above each of the peaks show where the $\Delta L=1$, $\Delta K=0,1$ transitions are expected to occur based on fits. The long vertical line is the hydrogenic frequency, 975.0545 cm^{-1}, of the $n=9$ to $n=17$ transition. The peaks with squares above them have been identified as $9G$-$17H$ transitions. The peaks with open circles above them are transitions with $\Delta L=-1$. The peaks with an X above them are unidentified transitions.

plotting the ion signal versus the laser angle, can be seen in Fig. 2, along with a fitted Gaussian peak used to obtain the line center. The 28 transition resonances observed in this study are illustrated in Fig. 3, and the transition frequencies are listed in Table I. The uncertainties listed there are due in part to the statistical errors from fits of the resonance lines, but the dominant source of uncertainty is the uncertainty in the actual laser frequency ν_L, which we estimate as ±30 MHz. During data collection, the laser was manually maintained near the center of the gain profile by adjusting the cavity length. The frequencies also have as another source of error the uncertainty in the calibration constants, $\beta=0.000\,713\,5(10)$ and $\theta_{perp}=184.460(34)°$, but since these result in highly correlated errors, they will be treated separately.

III. ANALYSIS

The 28 transitions consisted of four sets of seven transitions for each nL-$n'L'$ transition allowed by the selection rules $\Delta L=1$ and $\Delta K=1$ or 0. The observed energies of these seven transitions determine the relative positions of the four fine structure energy levels in $n=9$ and $n=17$. The four sets observed were the $9H$-$17I$, the $9I$-$17K$, the $9K$-$17L$, and the $9L$-$17M$. Figure 4 shows an energy level diagram of one such nL-$n'L'$ set and the seven transitions allowed by the selections rules.

The fine structure is modeled by a polarization potential

$$V_{pol} = -\left[\frac{e^2\alpha_S}{2r^4}+\frac{\eta}{r^6}+\cdots\right]-\left[\frac{eQ}{r^3}+\frac{\alpha_T}{2r^4}+\cdots\right] \times \frac{X_C^2\cdot C^2(\Omega_r)}{\begin{pmatrix} J_C & 2 & J_C \\ -J_C & 0 & J_C \end{pmatrix}}. \qquad (2)$$

In this equation, r is the radial coordinate of the Rydberg

TABLE I. List of the 28 transitions observed. Column 1 identifies each of the transitions using the nL_K notation. Column 2 gives the frequency at which the transition was observed. Column 3 lists the number of times each transition was observed. Column 4 gives the second-order energy contribution for the particular transition, and column 5 gives the relativistic energy contribution for the transition. Column 6 gives the transitions with the contributions applied. The transitions marked with an asterisk (*) or a dagger (†) indicate transitions which are unresolved.

Transition	ΔE_{obs} (cm^{-1})	No. of obs.	ΔE^2 (cm^{-1})	ΔE_{rel} (cm^{-1})	ΔE_{corr} (cm^{-1})
$9H_{7/2}$-$17I_{9/2}$	975.8918(10)	2	−0.0048	0.0007	975.8959(10)
$9H_{9/2}$-$17I_{9/2}$*	974.9448(10)	2	−0.0002	0.0007	974.9444(10)
$9H_{9/2}$-$17I_{11/2}$	975.0301(10)	2	−0.0009	0.0007	975.0303(10)
$9H_{11/2}$-$17I_{11/2}$	974.7658(10)	2	0.0021	0.0007	974.7631(10)
$9H_{11/2}$-$17I_{13/2}$	974.7855(10)	2	0.0020	0.0007	974.7829(10)
$9H_{13/2}$-$17I_{13/2}$	975.7366(10)	2	0.0047	0.0007	975.7312(10)
$9H_{13/2}$-$17I_{15/2}$	975.6522(10)	2	0.0048	0.0007	975.6468(10)
$9I_{9/2}$-$17K_{11/2}$	975.4879(10)	2	−0.0032	0.0005	975.4907(10)
$9I_{11/2}$-$17K_{11/2}$	974.9172(10)	2	0.0003	0.0005	974.9164(10)
$9I_{11/2}$-$17K_{13/2}$†	974.9703(10)	2	0.0001	0.0005	974.9697(10)
$9I_{13/2}$-$17K_{13/2}$	974.8378(10)	2	0.0010	0.0005	974.8363(10)
$9I_{13/2}$-$17K_{15/2}$	974.8481(10)	2	0.0010	0.0005	974.8467(10)
$9I_{15/2}$-$17K_{15/2}$	975.4223(10)	2	0.0014	0.0005	975.4205(10)
$9I_{15/2}$-$17K_{17/2}$	975.3670(10)	2	0.0013	0.0005	975.3652(10)
$9K_{11/2}$-$17L_{13/2}$	975.3044(10)	2	−0.0033	0.0003	975.3074(10)
$9K_{13/2}$-$17L_{13/2}$	974.9348(10)	2	−0.0002	0.0003	974.9347(10)
$9K_{13/2}$-$17L_{15/2}$†	974.9716(10)	2	−0.0001	0.0003	974.9714(10)
$9K_{15/2}$-$17L_{15/2}$	974.8983(10)	2	0.0003	0.0003	974.8977(10)
$9K_{15/2}$-$17L_{17/2}$	974.9050(10)	2	0.0003	0.0003	974.9044(10)
$9K_{17/2}$-$17L_{17/2}$	975.2767(10)	2	0.0005	0.0003	975.2759(10)
$9K_{17/2}$-$17L_{19/2}$	975.2388(10)	2	0.0004	0.0003	975.2380(10)
$9L_{13/2}$-$17M_{15/2}$	975.2140(10)	2	0.0002	0.0002	975.2136(10)
$9L_{15/2}$-$17M_{15/2}$	974.9592(10)	2	−0.0002	0.0002	974.9592(10)
$9L_{15/2}$-$17M_{17/2}$	974.9860(10)	2	−0.0001	0.0002	974.9859(10)
$9L_{17/2}$-$17M_{17/2}$	974.9402(10)	1	0.0001	0.0002	974.9398(10)
$9L_{17/2}$-$17M_{19/2}$*	974.9448(10)	2	0.0001	0.0002	974.9445(10)
$9L_{19/2}$-$17M_{19/2}$	975.1994(10)	1	0.0002	0.0002	975.1991(10)
$9L_{19/2}$-$17M_{21/2}$	975.1734(10)	2	0.0002	0.0002	975.1730(10)

electron and Ω_r represent its angular coordinates. The first terms in brackets are the scalar components of the potential, and the second terms in brackets are the tensor components. Higher-order terms are not taken into account. In the scalar component α_S is the dipole polarizability, and η contains information about the quadrupole polarizability and the nonadiabatic dipole polarizability. In the tensor components, Q is the quadrupole moment and α_T is the tensor polarizability. The energy levels of the Rydberg fine structure are given by

$$E = E_r^0 + \langle \psi_r^0 | V_{pol} | \psi_r^0 \rangle + \sum_{r'} \frac{|\langle \psi_r^0 | V_{pol} | \psi_{r'}^0 \rangle|^2}{E_r^0 - E_{r'}^0} + E_{rel}. \quad (3)$$

E_r^0 is the zeroth-order, purely hydrogenic energy of the atom. ψ_r^0 is the hydrogenic wave function of the Rydberg electron. The second term, the expectation value of V_{pol}, is the dominant contribution to the fine structure. The third term is a

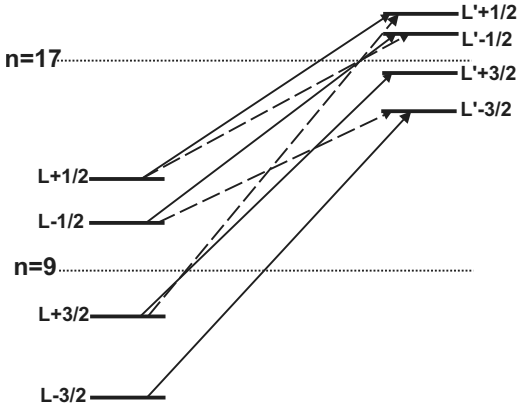

FIG. 4. Energy level diagram showing the seven dominant transitions in a $9L$-$17L'$ set. The solid lines are the $\Delta K=1$ transitions, and the dotted lines are the $\Delta K=0$ transitions. Notice that measuring the seven transition energies determines the relative positions of all eight levels.

TABLE II. Results of the fit to the scalar, vector, and tensor structure in argon. Column 1 lists the energy interval for which the fit was done. Column 2 gives the difference in the scalar coefficients. Column 3 gives the vector coefficient for the $n=9$ case. Column 4 gives the tensor coefficient for the $n=9$ case, and column 5 gives the tensor coefficient for the $n=17$ case. As expected, the A_2 coefficients for $n=17$ are about an order of magnitude smaller than those for $n=9$.

Energy interval	ΔA_0 (cm^{-1})	A_1 ($n=9$) (cm^{-1})	A_2 ($n=9$) (cm^{-1})	A_2 ($n=17$) (cm^{-1})
9*H*-17*I*	0.2614(9)	$8.0(8.5)\times10^{-5}$	−0.9498(10)	−0.0855(10)
9*I*-17*K*	0.1042(8)	$-0.2(9.0)\times10^{-5}$	−0.5738(14)	−0.0546(10)
9*K*-17*L*	0.0462(8)	$-2.2(5.8)\times10^{-5}$	−0.3720(11)	−0.0377(10)
9*L*-17*M*	0.0222(9)	$-1.9(2.0)\times10^{-5}$	−0.2546(10)	−0.0263(10)

small, second-order energy and is the effect due to mixing with all other possible Rydberg levels. These second-order energies have been calculated using the Dalgarno-Lewis method, similar to the second-order energy calculations for neon [13]. The relativistic effect E_{rel}, due to the p^4 term in the Rydberg electron's kinetic energy, is also small. By subtracting the small contributions of both these terms, a pattern due only to the first two terms in Eq. (3) is established:

$$\Delta E_{corr} = \Delta E_{obs} - \Delta E^{[2]} - \Delta E_{rel}, \tag{4}$$

where $\Delta E^{[2]}$ represents the contribution of the third term in Eq. (3).

This corrected energy can be written in terms of its scalar, vector, and tensor components, so

$$E_{corr} = E_0 + A_0 + A_1\{\vec{J}_C \cdot \vec{L}\} + A_2\{T^2_{J_C} \cdot T^2_L\}, \tag{5}$$

where

$$\{\vec{J}_C \cdot \vec{L}\} = \frac{1}{2}[K(K+1) - J_C(J_C+1) - L(L+1)] \tag{6}$$

and

$$\{T^2_{J_C} \cdot T^2_L\} = (-1)^{J_C+K}\begin{Bmatrix} K & L & J_C \\ 2 & J_C & L \end{Bmatrix}\frac{(2L+1)\begin{pmatrix} L & 2 & L \\ 0 & 0 & 0 \end{pmatrix}}{\begin{pmatrix} J_C & 2 & J_C \\ -J_C & 0 & J_C \end{pmatrix}}. \tag{7}$$

The scalar, vector, and tensor structure coefficients are A_0, A_1, and A_2, respectively. In the effective potential model above, A_1 is expected to be zero, but an experiment done in neon [4] showed that the vector structure is significant, so it was included here to see if it is significant in the fine structure of argon as well.

Since the transitions are actually energy differences between two levels in the fine structure, this can be written as

$$\Delta E_{corr} = \Delta E_0 + \Delta A_0 - (A_1)_n\{\vec{J}_C \cdot \vec{L}\}_{L,K} - (A_2)_n\{T^2_{J_C} \cdot T^2_L\}_{L,K} + (A_1)_{n'}\{\vec{J}_C \cdot \vec{L}\}_{L',K'} + (A_2)_{n'}\{T^2_{J_C} \cdot T^2_L\}_{L',K'}. \tag{8}$$

For the $n=17$ case, A_1 was set equal to zero for the fit, since the fine structure intervals within $n=17$ are much smaller than those of the $n=9$ states and the values of A_1 for $n=9$ were found to be very small. For each $nL-n'L'$ set, there are seven transitions and four fitting parameters. Four such sets of seven were observed to give four values of ΔA_0, four values of A_1, and eight values of A_2. Table II shows the fitted values for each of the ΔA_0, A_1, and A_2 coefficients. It can be seen that the values of A_1 for the $n=9$ case are indeed small. Also, the A_2 coefficients for $n=17$ are about an order of magnitude smaller than those for $n=9$. The probabilities of getting the reduced chi-squared values for each of the four fits were quite acceptable, so the statistical error of 0.0010 cm^{-1} for each of the transitions is reasonable. The parameter errors in Table II also include the effects of the systematic errors in the calibration constants β and θ_{perp}.

With these fitted coefficients, the scalar dipole polarizability and the quadrupole moment can be determined. The scalar component of the fine structure is given by

$$\Delta A_0 = \frac{-\alpha_S}{2}(\langle r^{-4}\rangle_{n,L} - \langle r^{-4}\rangle_{n',L'}) - \eta(\langle r^{-6}\rangle_{n,L} - \langle r^{-6}\rangle_{n',L'}) + \cdots . \tag{9}$$

Dividing this equation by $\Delta\langle r^{-4}\rangle = \langle r^{-4}\rangle_{n,L} - \langle r^{-4}\rangle_{n',L'}$, we can plot

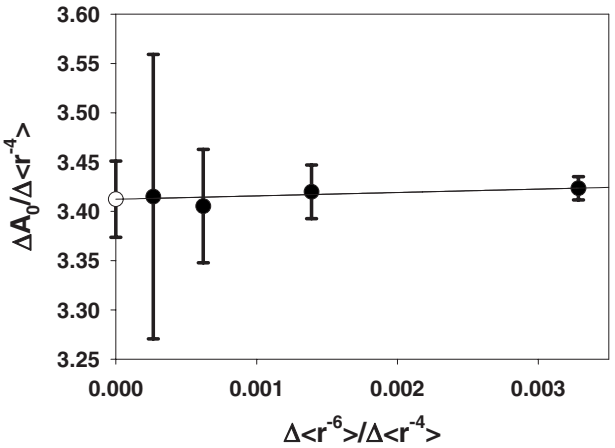

FIG. 5. A plot of the scalar coefficients normalized to $\Delta\langle r^{-4}\rangle$ vs $\Delta\langle r^{-6}\rangle/\Delta\langle r^{-4}\rangle$ for each of the four energy intervals. The y intercept is shown by the open circle and gives the value of half the dipole polarizability, $\alpha_S/2 = 3.412(38)a_0^3$.

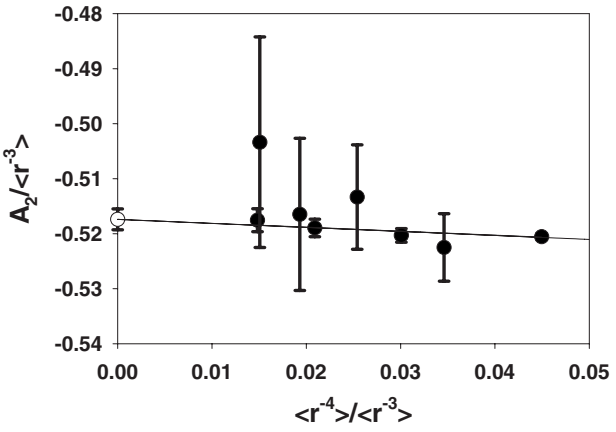

FIG. 6. A plot of the tensor coefficients normalized to $\langle r^{-3}\rangle$ vs $\langle r^{-4}\rangle/\langle r^{-3}\rangle$ for each of the eight tensor coefficients for both $n=9$ and $n=17$. The y intercept, shown by the open circle, is the quadrupole moment for Ar^+, $Q=-0.517(2)ea_0^2$.

$$\frac{\Delta A_0}{\Delta\langle r^{-4}\rangle} \quad \text{vs} \quad \frac{\Delta\langle r^{-6}\rangle}{\Delta\langle r^{-4}\rangle},$$

as shown in Fig. 5, where $\Delta\langle r^{-6}\rangle=\langle r^{-6}\rangle_{n,L}-\langle r^{-6}\rangle_{n',L'}$. The y intercept gives a value for $\alpha_S/2$, and the slope is η. If higher-order effects were important, there would be a curvature to the graph, which is not present. So, from this plot, the scalar dipole polarizability of Ar^+ is

$$\alpha_S = 6.83(8)a_0^3.$$

Also,

$$\eta = 3(12)e^2a_0^5,$$

which is consistent with zero.

The quadrupole moment can be determined in a similar manner with the tensor components of the effective potential. The tensor coefficient of the energy can be written

$$A_2 = -eQ\langle r^{-3}\rangle_{n,L} - \frac{\alpha_T}{2}\langle r^{-4}\rangle_{n,L} + \cdots . \tag{10}$$

Figure 6 shows a plot of

$$\frac{A_2}{\langle r^{-3}\rangle} = -eQ - \frac{\alpha_T}{2}\frac{\langle r^{-4}\rangle}{\langle r^{-3}\rangle}. \tag{11}$$

The y intercept gives the quadrupole moment, and the slope is α_T. The quadrupole moment was found to be

$$Q = -0.517(2)ea_0^2,$$

and the tensor dipole polarizability is

$$\alpha_T = -0.07(5)a_0^3.$$

Also, since the A_1 values are consistent with zero, no evidence of vector structure is found in this experiment. This is not surprising given the level of precision. The magnetic interactions, which dominate in neon, would be expected to give a value of $A_1 \approx 2\alpha^2\langle r^{-3}\rangle/3$ or $A_1 \approx 6\times10^{-5}$ cm^{-1} for the $9H$ state. We are unaware of any theoretical calculations of either α_S or Q that could be compared with these results.

IV. CONCLUSION

By taking measurements of the optical transitions between the $n=9$ and $n=17$ energy levels in Rydberg atoms of argon, the dipole polarizability and the quadrupole moment of Ar^+ were found to within about 1% precision. Within the precision of this study no significant vector component of the fine structure pattern was found. Higher-precisions studies using microwave methods will be necessary to determine whether or not argon has a vector structure similar to that found in neon.

ACKNOWLEDGMENTS

This work was supported by the Chemical Sciences, Geosciences, and Biosciences Division of the Office of Basic Energy Sciences, Office of Science, U.S. Department of Energy.

[1] S. R. Lundeen, in *Advances in Atomic, Molecular, and Optical Physics*, edited by Chun C. Lin and Paul Berman (Academic Press, 2005), Vol. 52, pp. 161–208.
[2] G. D. Stevens and S. R. Lundeen, Phys. Rev. A **60**, 4379 (1999).
[3] R. F. Ward, Jr., W. G. Sturrus, and S. R. Lundeen, Phys. Rev. A **53**, 113 (1996).
[4] P. L. Jacobson, R. D. LaBelle, W. G. Sturrus, R. F. Ward, Jr., and S. R. Lundeen, Phys. Rev. A **54**, 314 (1996).
[5] E. L. Snow, M. A. Gearba, R. A. Komara, S. R. Lundeen, and W. G. Sturrus, Phys. Rev. A **71**, 022510 (2005).
[6] W. G. Sturrus, E. A. Hessels, P. W. Arcuni, and S. R. Lundeen, Phys. Rev. A **44**, 3032 (1991).
[7] P. L. Jacobson, R. A. Komara, W. G. Sturrus, and S. R. Lundeen, Phys. Rev. A **62**, 012509 (2000).
[8] R. A. Komara, M. A. Gearba, C. W. Fehrenbach, and S. R. Lundeen, J. Phys. B **38**, S87 (2005).
[9] R. A. Komara, M. A. Gearba, S. R. Lundeen, and C. W. Fehrenbach, Phys. Rev. A **67**, 062502 (2003).
[10] W. Clark, C. H. Greene, and G. Miecznik, Phys. Rev. A **53**, 2248 (1996).
[11] B. Zygelman, Phys. Rev. Lett. **64**, 256 (1990).
[12] W. Clark and C. H. Greene, Rev. Mod. Phys. **71**, 821 (1999).
[13] R. A. Komara and W. G. Sturrus, Phys. Rev. A **58**, 521 (1998).